Chapter 6

Enhancement of dielectric and magnetic properties of $0.5BaFe_{12}O_{19}$-$0.5Bi_{2/3}Cu_3Ti_4O_{12}$ nanocomposite synthesized via chemical route

6.1. Introduction

Nanosized ferrite materials have been widely used to synthesize bulk materials to achieve desired properties such as dielectric, electrical and magnetic properties, suitable for industrial applications. The electric and dielectric properties of these ferrites are mainly due to low dielectric loss, low eddy current, high saturation magnetization and higher resistivity. These properties of material make them suitable for device applications such as antenna, memory chips, automobiles, telecommunications and energy storage etc. There is another important class of transition metal oxides namely Fe_2O_3, Fe_3O_4 and other few other oxides which possess the magnetic properties such as high permeability and high Q making these materials suitable for oscillators, modulators, resonators and biomedical applications. Because of this wide range of applicability, the extensive work has been done in the last decades to improve properties of these ferrites using the substitution of transition metal ions [Du *et al.* (2010), Patil *et al.* (2017)].Various transition metal oxides or alkaline earth metal oxides are substituted with the ferrite to enhance the desirable electrical properties. The continuous demands of electronic devices such as televisions, mobile phones and computers for human requirement create a new type of environmental pollution referred as electromagnetic interference (EMI). Such types of pollution have an adverse affect on human tissue and causes cancer. Therefore, researchers have been made an attempt to synthesize nanomaterials and nanocomposites for reducing to EMI pollution. Furthermore, ferrites have been widely studied and most suitable material candidate to control the EMI pollution due to possession of poor dielectric loss. In addition, due to high coercivity and impedance matching, these materials have damaging performance of EMI pollution [Pubby *et al.* (2017), Kaur *et al.* (2017)] Previous literature showed that the hexaferrite nanocomposite materials have been widely attracted towards to reduce their shielding

performance due to their excellent magnetic properties [Mohammed *et al.* (2018)].As a new class of hexagonal ferrites having the molecular formula $MFe_{12}O_{19}$ (where M = Ba, Sr, Ca and Pb) show strong ferrimagnetism [Roshanaei *et al.* (2018)].The M-type barium hexaferrite ($BaFe_{12}O_{19}$) is a hard-magnetic material, having hexagonal magnetoplumbite structure with space group $P6_3/mmc$ [El Shater *et al.* (2018)].The magnetic behavior of these oxides arises due to the presence of high Curie temperature. The barium hexaferrite, $BaFe_{12}O_{19}$ has high saturation magnetization, high coercivity, high chemical stabilities, corrosion resistance as well as high magneto-crystalline anisotropy [Singhal *et al.* (2018), Onreabroy *et al.* (2012), Xie *et al.* (2013), Zhao *et al.* (2016), Zhao *et al.* (2015)].Therefore, it has wide applications such as high magnetic recording media, loudspeakers, ferrofluids, sensors, the rotors in small DC motors [Ashiq *et al.* (2017), Xu *et al.* (2011), Anbarasu *et al.* (2013)].The magnetic and electrical properties of barium hexaferrite are strongly dependent on the microstructure and morphology of the oxide. Morphologies are controlled by parameters used in synthesis, sintering duration, temperature and annealing atmospheres [Singh *et al.* (2014), Hong *et al.* (2015)].The magnetic properties of these hexagonal ferrites can be improved by the partial substitution of metal cations at the iron (Fe^{+3}) site in the barium hexaferrite and addition of some metal oxides such as SiO_2, Bi_2O_3 [Mudsainiyan *et al.* (2014), Li *et al.* (2002), Namura and Hankui (2003), Zhang *et al.* (2002)].The magnetic properties also enhanced in various composites of ferrites such as $CoFe_2O_4/BaTiO_3$, ferrite/lead-zirconate-titanate (PZT),$CoFe_2O_4$–$BaTiO_3$, $BaFe_{12}O_{19}$–$BaTiO_3$, have also demonstrated strong magnetostriction effects [Lou *et al.* (2009), Liu *et al.* (2009), Walther *et al.* (2016), Trivedi *et al.* (2015)].The phenomenon of multiferroicity in $BiFeO_3$ and $BiMnO_3$ materials has been reported earlier where Mn^{+3} and Fe^{+3} ions responsible for magnetism whereas Bi^{+3} non-cetrosymmetric ion developed ferroelectricity in materials [Dutta *et al.* (2014),

Dutta *et al.* (2013), Dutta *et al.* (2010), Kimura *et al.* (2003)]. Therefore, there is continuous demand for new composite materials which shows multiferroicity in which magnetic field can be controlled by the electric field and vice versa. In addition to this, $Bi_{2/3}Cu_3Ti_4O_{12}$ (BCTO) shows similarity to $CaCu_3Ti_4O_{12}$ like-compound having cubic perovskite type of structure with lattice constant a=7.413 Å and space group of Im3. In the BCTO, Bi ion occupied 1/3 position of vacant orbital to attain charge neutrality which influence the dielectric behavior of the material. The reported value of dielectric constant at 25 °C and 10^5 Hz observed for BCTO is1871. However, this value is very low compared to that of CCTO compound as reported by Subramanian et al [Subramanian and Sleight (2002), Liu *et al.* (2004)]. The higher value of dielectric constant arises due to reduction in size of the ferroelectric materials which are also tunable with the application of a modest voltage. The voltage tunability and the low cost are advantageous in the modern trends for many applications, such as tuner devices, dehydration, sterilization, pasteurization, tempering (thawing), blanching, and cooking. There is limited work done on the hexagonal ferrites with BCTO type of perovskite material systems [Kanai *et al.* (2001), Mantese *et al.* (1996)]. The objective of this work was to synthesize and fabricate 0.5$BaFe_{12}O_{19}$–0.5$Bi_{2/3}Cu_3Ti_4O_{12}$ (BHF–BCT) nanocomposite via chemical route at the lower sintering temperature for enhancement of their dielectric as well as magnetic properties of the nanocomposite material.

6.2. Experimental

6.2.1 Synthesis

The nanocomposite 0.5$BaFe_{12}O_{19}$–0.5$Bi_{2/3}Cu_3Ti_4O_{12}$ (BHF–BCT) was synthesized via chemical route in two steps. Analytical grade chemicals of barium nitrate, Ba $(NO_3)_2$(99.5% Merck, India), iron nitrate, Fe $(NO_3)_3$.$9H_2O$ (98% Merck, India) were taken as starting materials for the

synthesis of $BaFe_{12}O_{19}$. The stoichiometric ratio of Ba and Fe metal nitrates were dissolved in distilled water in a beaker. Secondly, $Bi_{2/3}Cu_3Ti_4O_{12}$ (BCTO) ceramic was prepared by the semi-wet route by dissolving the stoichiometric amount of bismuth nitrate, $Bi(NO_3)_3 \cdot 5H_2O$ (99.5%, Merck, India), copper nitrate, $Cu(NO_3)_2 \cdot 3H_2O$ (99.8%, Merck, India) in a beaker. The solid TiO_2 (99.9%, Merck, India) is not dissolved in water, so the fine powder of it was added to the beaker. The citric acid (per equivalent to metal ion) was added in the both reaction mixtures which facilitates the self-combustion. Both the reaction mixtures were heated on hot plate at 343 – 353 K to evaporate the excess water. A fluffy mass of BHF and BCTO were obtained. The obtained resulting powders were calcined separately at 1073 K for 8 h. For the fabrication of the BHF–BCT composite, an equal molar ratio of BHF and BCTO component were thoroughly grounded (24 h) in an agate and mortar in solvent medium of ethanol. The cylindrical pellets (11.5 mm × 1.00 mm) were formed with the help of hydraulic press using PVA as a binder by applying pressure of 4 tons. The pellets were heated to 773 K for 2 h to remove the binder. Finally, the composite was sintered in electrical tube furnace at 1173 K for 8 h in air.

6.2.2 Characterization

The crystalline nature of sintered BHF–BCT nanocomposite was characterized by X-ray diffraction analysis (Rigakuminiflex 600, Japan) employing Cu-Kα radiation (λ = 1.54 Å) in the range of $20° \leq 2\theta \leq 80°$ with scan rate 2°/min. The particle size of the nanocomposite was investigated by a transmission electron microscope (TEM, FEI TECANI G^2 20 TWIN; USA). The surface morphology of BHF–BCT nanocomposite was analyzed by scanning electron microscope (ZEISS, model EVO–18 research; Germany). The elemental compositions of the nanocomposite were examined by Energy dispersive X-rays (EDX) spectroscopy (Oxford instrument; USA) attached with SEM instrument. The surface roughness of the composite was

analyzed by atomic force microscopy (AFM, NTEGRA prima, Germany). Magnetic measurement was carried out using a Quantum Design MPMS-3 over a temperature range 5–300 K and applied magnetic field of ± 2 T. In addition, temperature dependent zero field cooling (ZFC) and field cooling (FC) magnetization were performed by SQUID VSM (vibrating sample magnetometer) dc in the temperature range 5 –300 K and applied magnetic field (100 Oe). Silver coated cylindrical pellets were used for the measurement of dielectric and electrical properties of the BHF–BCT nanocomposite with the help of LCR meter (PSM 1735, NumetriQ 4thLtd. U.K.) with the variation of frequency (100 Hz–5 MHz) and temperature (300–500 K).

6.3. Results and discussion

6.3.1. Microstructural Studies

The bulk densities of BHF- BCT nanocomposite obtained by Archimedes technique at a different temperature is shown in Figure 6.1.

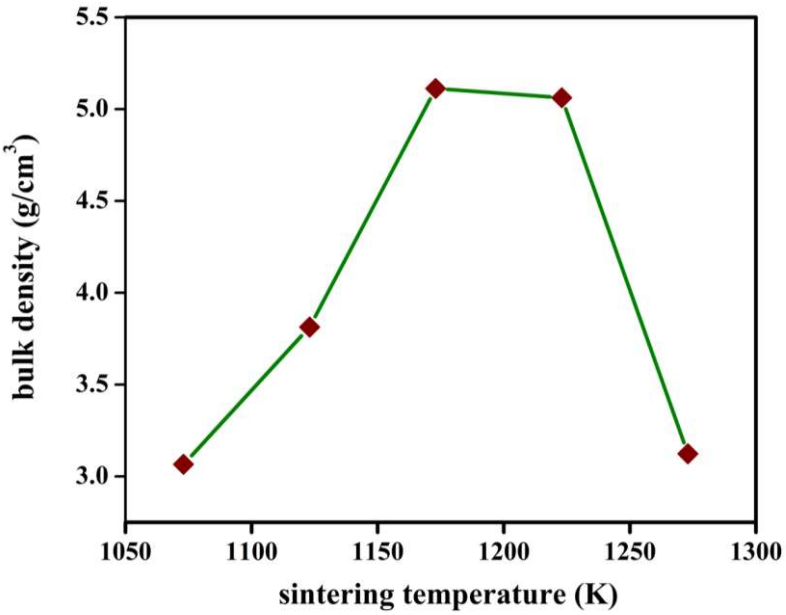

Figure 6.1 Plots of bulk densities with sintering temperature of BHF-BCT nanocomposite.

The figure reveals that the density of nanocomposite increases rapidly with increasing temperature up to the temperature 1173 K, and after that it decreases steadily up to 1223 K and sharply decreases beyond 1223 K. The maximum densification of the nanocomposite is observed at 1173 K which indicates the minimum porosity. It is also observed that further porosity increases on increasing the temperature of the material. The approximate value of the bulk density obtained by the plots is found to be 5.10 g/cm^3 at the sintering temperature of 1173 K for 8 h, which is lower than the theoretical density (6.45 g/cm^3) obtained by the XRD results.However, only 79.06 % densification is observed from the comparison of calculated and theoretical density after sintering of the materials at 1173 K for 8 h. This densification value is achieved due to particle size or compression pressure and 100 % densification may be obtained by reduction of particle size to nano- size or submicron of BCT-BHF powder [Nie *et al.* (2015), Sardjono and Djauhari (2016)].

Figure 6.2 (a) and (b) show the XRD patterns of calcined and sintered BHF–BCT nanocomposite sintered at 1073 and 1173 K for 8 h, respectively. All the X-ray diffraction peaks of the sintered materials are belonging to the parent materials of $BaFe_{12}O_{19}$ (JCPDS- 78–0132) and $Bi_{2/3}Cu_3Ti_4O_{12}$ (JCPDS- 80–1343) which confirmed the formation of nanocomposite consisting the pure phase of the parent materials. The average crystallite size of the nanocomposite was determined by the Debye- Scherrer formula using the intense peak of the XRD patterns [Khare *et al.* (2017)].

$$D = \frac{k\lambda}{\beta \cos\theta} \qquad (6.1)$$

where,D is the crystallite size, k is the constant value taken as 0.90, λ is the wavelength of X-ray, θ is the Braggs angle, and β is the peak width of the diffraction peak at half-maxima (FWHM) in radians.

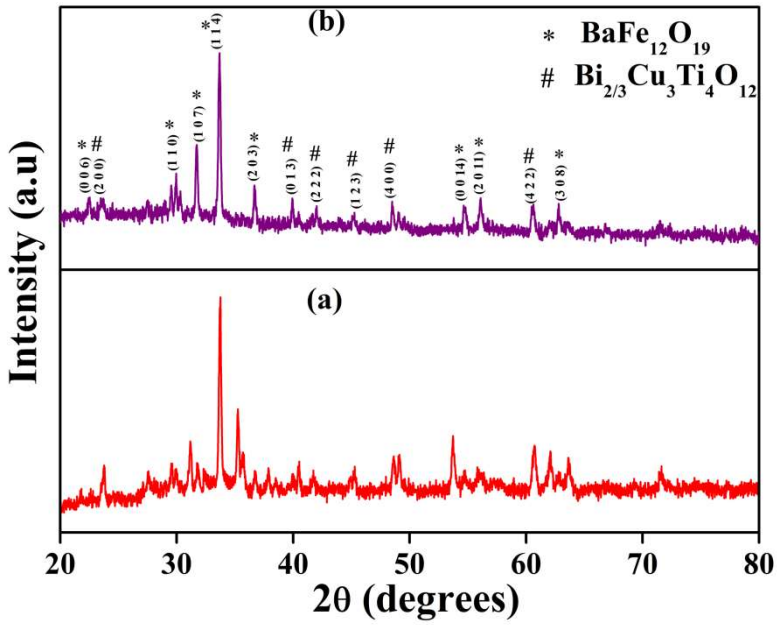

Figure 6.2 X-ray diffraction pattern of BHF-BCT nanocomposite (a) calcined at 1073 K and (b) sintered at 1173 K for 8 h, respectively.

The β is corrected value of diffraction peak due to instrumental broadening for crystallite size concerning standard silicon wafer sample. The crystallite size of the nanocomposite ceramic was measured by using the corrected value of FWHM (β). The average crystallite size of BHF–BCT nanocomposite is found to be 53 ± 5 nm.

Figure 6.3 shows the Le-Bail full pattern well matched with the XRD analysis using Fullprof software.

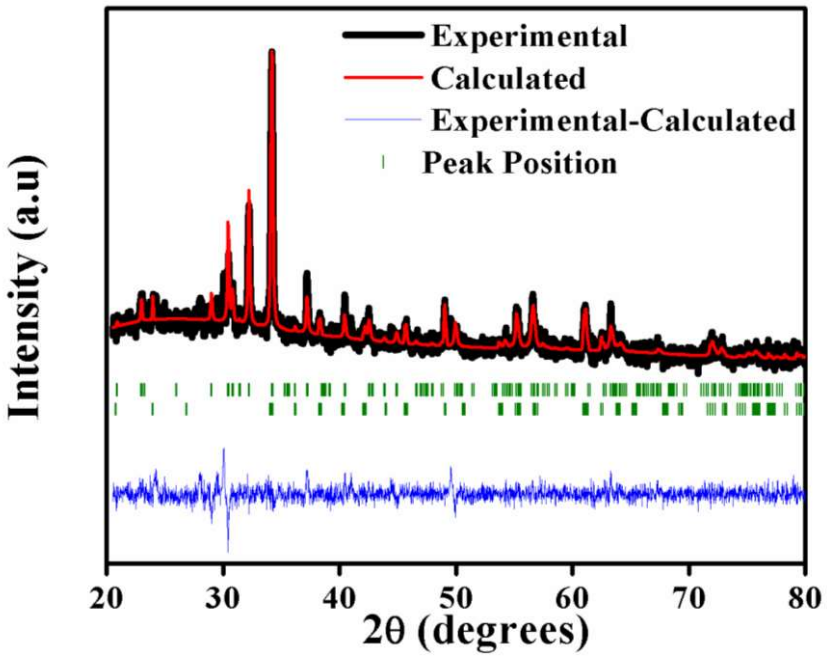

Figure 6.3 Le-bail analysis of XRD patterns for BHF–BCT nanocomposite sintered at 1173 K for 8 h. The black line demonstrates experimental, red line represents calculated, Blue line indicates the difference between experimental and calculated diffraction patterns and vertical tick marks in the second and third rows represent peak positions.

The experimental data of BHF–BCT nanocomposite confirmed the phases of the parent materials of BHF and BCT, hexagonal and orthorhombic structure with space group P6$_3$/*mmc* and Pnma, respectively. The refined lattice parameters of the nanocomposite are listed in table 6.1. The observed lattice parameters are in good agreements with hexagonal barium hexaferrite as reported earlier [Kumar *et al.* (2019)].

Table 6.1 Refined lattice parameters, Angles, Bragg R-factor and RF-factor for 0.5BaFe$_{12}$O$_{19}$–0.5Bi$_{2/3}$Cu$_3$Ti$_4$O$_{12}$ (BHF–BCT) nanocomposite.

χ^2 = 3.10	Phase-1	Phase-2
	$BaFe_{12}O_{19}$ (BHF)	$Bi_{2/3}$ $Cu_3Ti_4O_{12}$ (BCT)
	Space group- $P6_3/mmc$	Space group -Pnma
Cell parameters	a = b= 5.878133Å, c = 23.240976 Å	a =5.395633Å, b =7.359714Å, c =5.250222 Å
Angle	α = β = 90°, γ =120°	α = β = γ= 90°
Bragg R-factor:	3.234	Bragg R-factor: 5.701
RF-factor :	2.877	RF-factor : 4.183

Figure 6.4 shows the FTIR spectrum of BHF–BCT nanocomposite recorded in the frequency range of 500–1500 cm^{-1}.

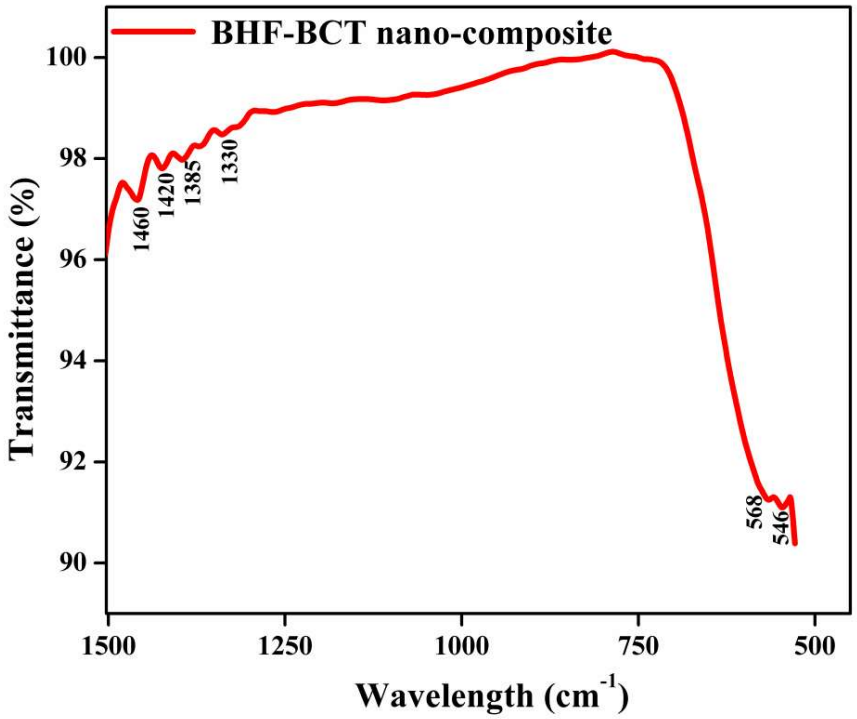

Figure 6.4 FTIR spectrum of BHF-BCT nanocomposite synthesized at 1173 K for 8 h.

The absorption bands appear at 530 cm^{-1}, and 560 cm^{-1} corresponds to octahedral and tetrahedral sites, respectively and displays the characteristic peaks of hexaferrite. The presence of Fe–O–Fe bonds is also confirmed due to the presence of an absorption band in the frequency range 1100–1500 cm^{-1} for BHF ceramic [Gordani *et al.* (2014)].The metal-oxygen (Bi-O) bonds in BCTO ceramic are due to asymmetric vibrations appearing in 1300–1500 cm^{-1}. The bands observed between 525 and 585 cm^{-1} confirm the presence of Cu–O bonds [Gautam *et al.* (2016)].The stretching frequencies corresponding to metal-oxygen bonds and metal-oxygen-metal bonds support the composite formation of the materials.

The bright field TEM images of BHF–BCT nanocomposite are shown in Figure 6.5(a) and (b) which reveals the presence of bimodal faceted particles. The average particles size is found to be 31 ± 5 nm. Figure 6.5(c) shows the selected area electron diffraction (SAED) pattern having spots on the ring which indicates the nanocrystalline nature of the composite. The zone axis of the diffraction pattern containing the planes (1 0 4), (1 1 6) and (4 4 2), (1 3 6) are found to be $[\bar{4}\,\bar{2}\,3]$, $[\overline{18}\ \overline{22}\ 8]$, respectively. Figure 5(d) shows high-resolution TEM image, the calculated inter-planer distance (d) are 2.68 Å and 1.61 Å correspond to (1 1 4), (2 1 8) planes for BHF ceramic and d for BCTO is 2.14 Å corresponding with (2 2 2) plane. These results are also substantiated with the above XRD results of JCPDS card number – 78–0132, 80–1343, respectively [Singh *et al.* (2013)].

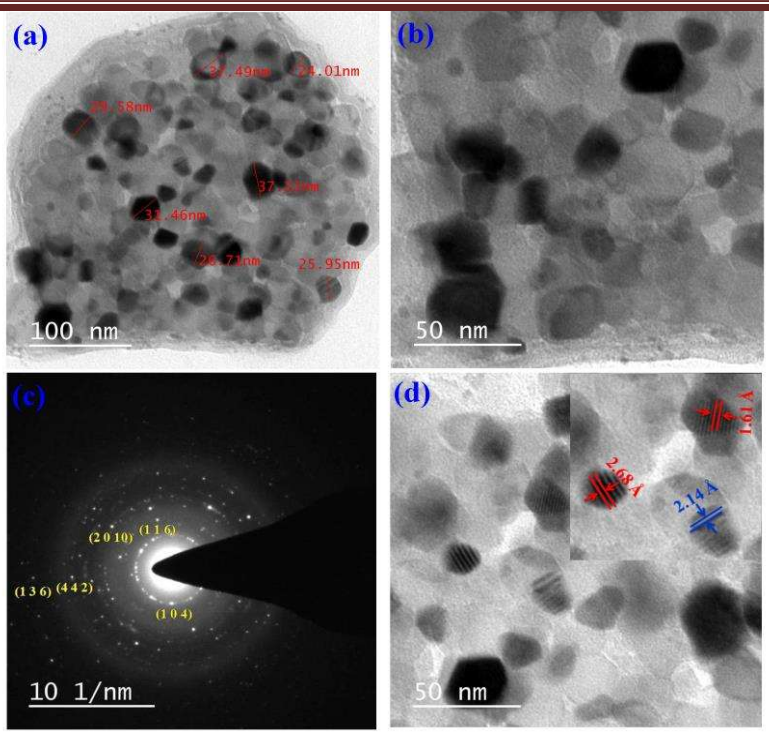

Figure 6.5(a and b)show bright field TEM images (c) High-resolution TEM image corresponding to their d spacing (d) selected area diffraction (SAED) pattern of BHF–BCT nanocomposite.

Figure 6.6(a) shows the SEM image of BHF–BCT nanocomposite sintered at 1173 K for 8 h. Nanocomposite displays the bimodal structure with hexagonal as well as round shape of the grains. The average grain size of BHF–BCT nanocomposite is found to be 700 ± 5 nm. Figure 6.6 (b) shows EDX spectra of the nanocomposite which reveals the presence of Ba, Fe, Bi, Cu, Ti and O elements with their atomic percentage of 1.43, 18.23, 2.11, 8.3, 8.28 and 64.66, respectively. The atomic percentages and existence of these elements in EDX spectra are also supported by energy dispersive mapping as shown in Fig. 6(c – h). Each element is represented

by separate color (mapping) and its uniform distribution indicated that the homogeneous distribution of the elements in the nanocomposite.

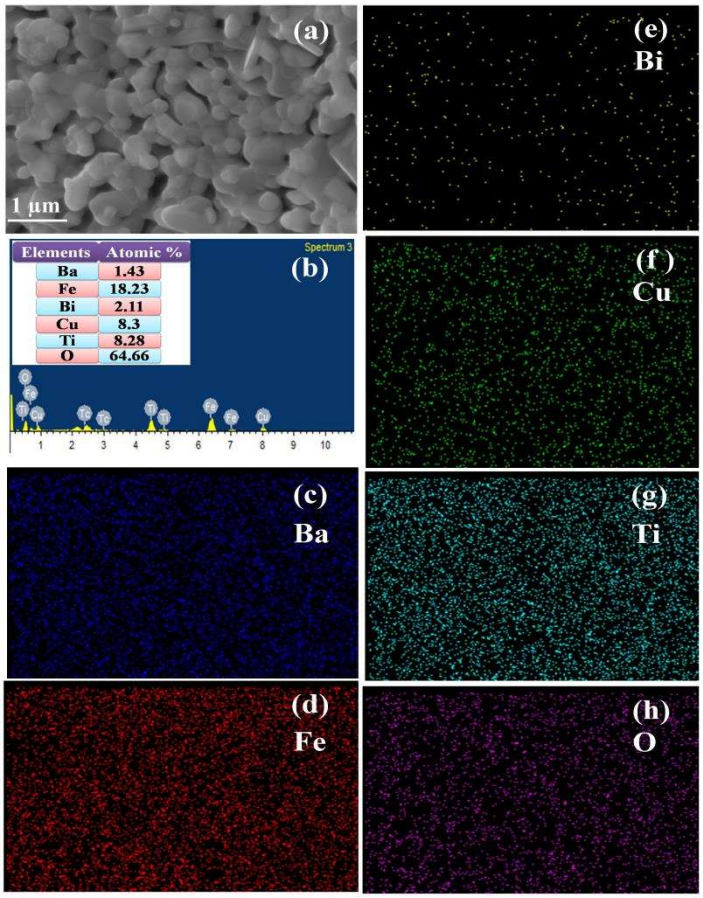

Figure 6.6(a) SEM image (b) Energy dispersive X-ray (EDX) spectrum for elemental composition and (c) – (h) EDX mapping of indivisible elements related with BHF–BCT nanocomposite sintered at 1173 K for 8 h.

AFM micrographs BHF–BCT nanocomposite sintered at 1173 K for 8 h is shown in Figure 6.7. The surface roughness (R_q) for 2D and the 3D image is estimated by following formula [Khare *et al.* (2018)].

$$R_q = \sqrt{\left(\sum \frac{(Z_i - Z_{ave})^2}{N}\right)} \qquad (6.2)$$

where, R_q is the surface roughness, Z_i is the height value at that point, Z_{ave} is the average of the Z values within the particular field, and N is the number of points within the given area.

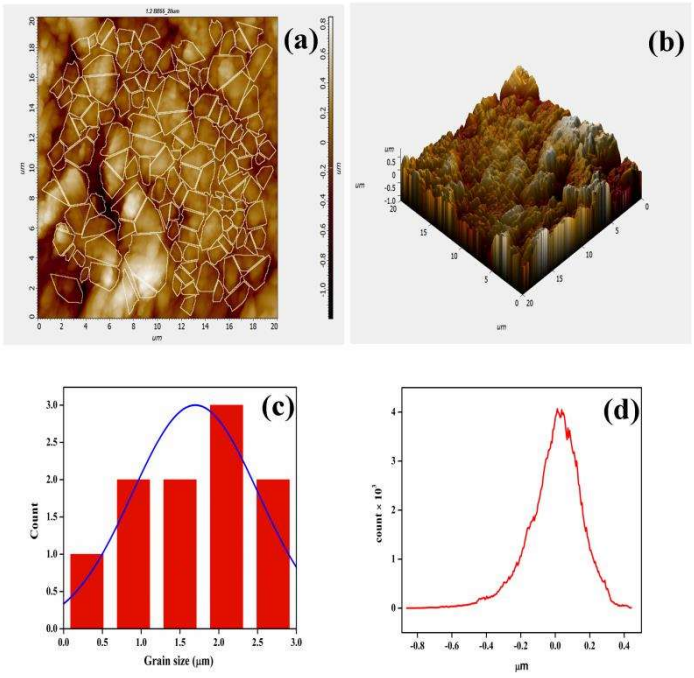

Figure 6.7 Atomic force microscopy (AFM) images (a)two dimensional for grain and grain boundaries (b)3D for roughness of particles (c) Histogram graph for particle size distribution and (d) peak distribution curve for grain roughness.

Figure 6.7(a) shows the AFM image of nanocomposite indicates the heterogeneous distribution of grains which are separated by the grain boundaries. From the AFM spectra (Figure 6.7(b)) grains are analyzed and some important information is withdrawn, such as root mean square roughness (R_q), average roughness (R_a), maximum area peak height (S_p) and maximum area valley depth (S_v) are found to be 0.261, 0.198, 0.842 and 1.188 μm, respectively on scanned area 20 μm × 20 μm. Figure 6.7(c) shows the histogram for 3D AFM image which indicates that the majority grains are in the range of 1.8–2.9 μm, whereas average grain size obtained by the plot is 1.0 ± 0.5 μm which is also supported by SEM [Gautam *et al.* (2017)].

Figure 6.7(d) shows the maximum profile peak height (R_p), root-mean-square roughness, (R_q), maximum profile valley depth (R_v) are obtained by peak the distribution of the 2D image, is found to be 0.319, 0.195 and 0.642 µm, respectively.

6.4. Ferroelectric Properties

The variation of electrical polarization with the electric field (P–E) hysteresis loop measured at 50 Hz at few selected temperatures under the electric field 5 kV/cm are shown in Figure 6.8.

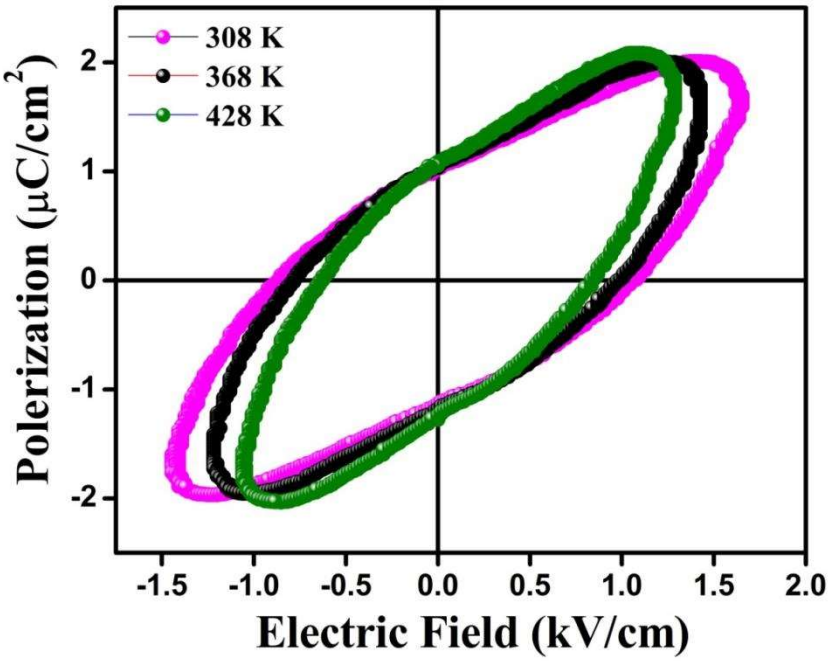

Figure 6.8 P–E unsaturated hysteresis loop of BHF–BCTO nanocomposite at few selected temperatures.

The values of remnant polarization (P_r) and coercivity (E_c) are calculated at few selected temperatures and mentioned in table 6.2. It is observed from the table that the value of remnant polarization and coercivity decrease with increasing temperature. The decrease in both of these polarizations may be lead to switching of domain motion and reversal of induced electric field

with increasing temperature considered as a thermally activated process. The absence of saturation polarization (P_s) indicates lossy capacitor nature of the BHF–BCT nanocomposite [Patel et al. (2016)].

Table 6.2 Remnant polarization (P_r) and Coercivity (E_c) of BHF-BCT composite at different temperatures.

Temperature (k)	Remnant polarization ($\mu C/cm^2$)	Coercivity (kV/cm)
318	1.038	1.072
328	1.035	0.993
338	1.036	0.817

6.5 Magnetic studies

Figure 6.9(a) shows the magnetic properties of BHF–BCT nanocomposite referring the Zero fields cooled magnetization (M^{ZFC}) and field cooled magnetization (M^{FC}) versus temperature recorded at 100 Oe. Both ZFC and FC curve does not converge to each other over a wide range of temperature which shows magnetic interaction due to strong coupling in the nanocrystals. Furthermore, FC curve attains maximum value and step like transition occurs in the zero fields cooled (ZFC) curve when temperature is lowered below T_M=170 K of the BHF-BCT nanocomposite [Lin *et al.* (2009)]. Figure 6.9(b) shows the M-H hysteresis plots of BHF–BCT nanocomposite at 5 and 300 K temperatures and magnetic field of ±2 T. Saturation magnetization (M_s) and remnant magnetization (M_r) increased with the decrease of temperature due to spin canting, surface effects or inhomogeneity of the nanocomposite [Issa *et al.* (2013), Xie *et al.* (2014), Zhao *et al.* (2014)].Surface effects can lead to increase or decrease the

saturation magnetization of the nanoparticles was reported earlier [Kodama *et al.* (1999), Respaud *et al.* (1998)].

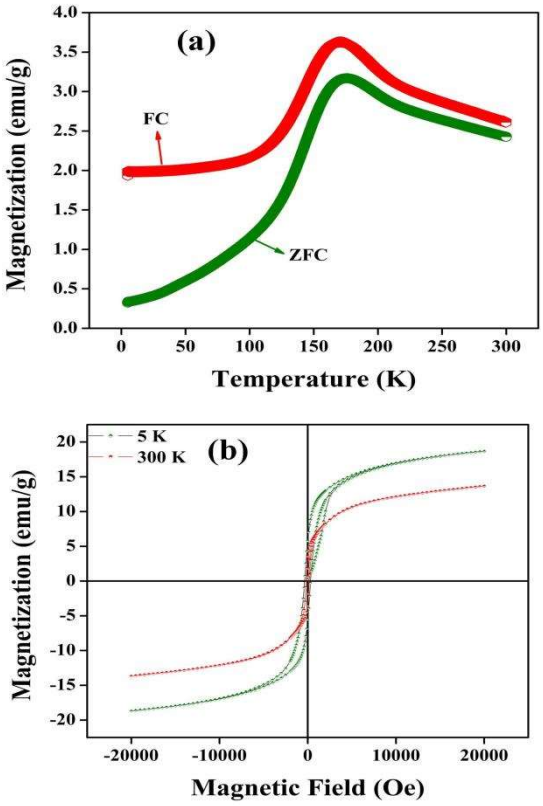

Figure 6.9(a) Temperature-dependence of Zero cooled field (ZFC) and Field cooled (FC) at H=100 Oe and ±2 T (b) M-H hysteresis curve of BHF–BCT nanocomposite at two different temperature (5 and 300 K).

The decrease in saturation magnetization of the materials due to surface magnetism arises in the case of clean surface was studied by Binder [Binder and Hohenberg (1976)] The coercivity (H_c) value of BHF–BCT nanocomposite calculated at 5–300 K by hysteresis plots are found to be 2.3 × 10^4 and 1.6 × 10^4 Ampere/meter, respectively which is lower than pure barium hexaferrite ($BaFe_{12}O_{19}$) [Issa *et al.* (2013)].The reduction in the value of coercivity for BHF–BCT nanocomposite than pure barium hexaferrite as reported earlier due to structural defect in

the materials because some of the hexagonal particles exist in the nanocomposite and also due to the contribution of non-magnetic BCTO phase with round shape of the particles in the materials [Kubo *et al.* (1985)]. Therefore, these composite have a weak net magnetic moment and exhibits weak ferromagnetism [Kumar *et al.* (2019), Lorenz *et al.* (2014)].The saturation magnetization (M_s), remnant magnetization (M_r) and coercivity (H_c) values of BHF–BCT nanocomposite are listed in table 6.3.

Table 6.3 Magnetic parameters of BHF-BCT nanocomposite at two different temperatures.

T (K)	M_s (emu/g)	M_r (emu/g)	M_r/M_s	H_c (A/m)
5	15.81	6.53	0.477	2.3×10^4
300	11.14	4.12	0.491	1.6×10^4

Figure 6.10 shows the variation of inverse magnetic susceptibility (χ) with temperature and applied the magnetic field (H=100 Oe) to validate the resulting data with Curie–Weiss law. The Curie–Weiss relation is expressed as the following Equation 6.3.

$$\chi^2 = \frac{C(x)}{T-\theta(x)} \quad (6.3)$$

Where, χ, C(x) and θ(x) are magnetic susceptibilities, Curie-Weiss constant and Curie-Weiss temperature, respectively. It is observed from the figure that the negative and positive slope. appeared with increasing temperature. Both the slopes meet at 165 K. This transition temperature is known as N′eel temperature (T_N). At this temperature, materials magnetic properties change from ferromagnetic in to paramagnetic. The value of T_N and θ(x) of the composite are calculated from the figure and found to be 165 K and -80.597 K, respectively.

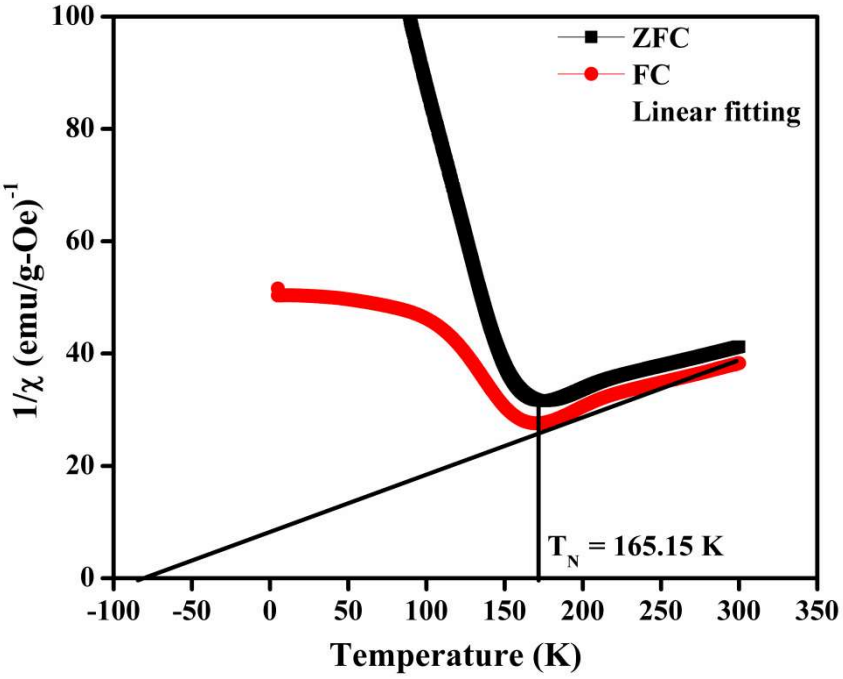

Figure 6.10 Temperature dependent inverse magnetic susceptibility at H= 100 Oe of the BHF–BCT nanocomposite.

The negative value of θ(x) indicates the antiferromagnetic behavior of the BHF-BCT nanocomposite. The magnetic spins of the materials are blocked below this temperature (T_N) [Hamad *et al.* (2016)].

6.6. Dielectric studies

Temperature-dependent dielectric constant [real (ε′); imaginary (ε″)] and tangent loss (tan δ) of BHF–BCT nanocomposite at 1 kHz, 10 kHz, and 100 kHz are shown in Figure 6.11. The value of dielectric constant increases to attain maxima and then decreases on increasing temperature. These maxima around 420 k is critical temperature representing phase transition from ferroelectric to paraelectric is shown in Figure 6.11(a) and (b). The value of critical temperature shifted towards higher temperature with increasing frequencies.

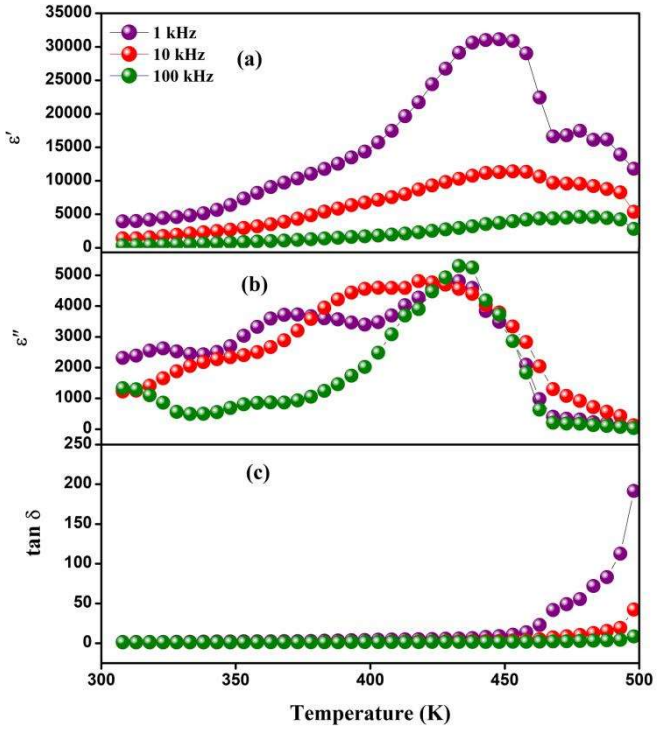

Figure 6.11 Plots of (a) real (ε′) (b) imaginary (ε″) dielectric constant and (c) tangent loss (tan δ) vs temperature at few selected frequencies of BHF–BCT nanocomposite.

This type of behavior observed in the materials indicates thermally activated process described in various earlier reports [Małecki *et al.* (2014)].The dielectric loss (tan δ) remains constant from 300–450 K, after that it increases with an increase of temperature as represented in Figure 6.11(c). The sharp increase of tan δ at the higher temperature may be due to charge accumulation at the interface of grains and grain boundaries [Ishiwata *et al.* (2011)].

Figure 6.12 shows the frequency dependent dielectric constant of real (ε′), imaginary (ε″) and dielectric loss (tan δ) of the BHF–BCT nanocomposite at a few selected temperatures. It is clear from the Figure 6.12(a) that the dielectric constant decreases with increasing frequency from 100 Hz to 100 kHz and then remains constant up to 5 MHz.

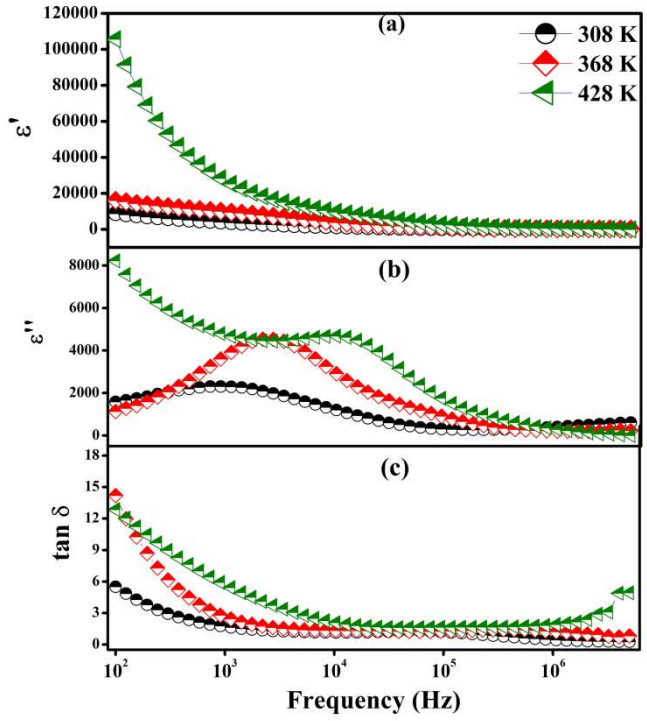

Figure 6.12 Variation of (a) real (ε′) (b) imaginary (ε″) part of dielectric constant dielectric constant and (c) dielectric loss (tan δ) vs frequency at few selected temperatures.

The increase in the dielectric constant of the real part (ε′) with frequency may be due to space charge polarization and the chemical micro-heterogeneities present in the materials [George *et al.* (2007)].The highest value of dielectric constant for BHF–BCT nanocomposite is found to be 10.7×10^4 at 100 Hz, and 428 K. Figure 6.12(b) exhibits the presence of relaxation peaks which shifted towards higher frequency region on increasing temperature which supports the presence of Maxwell Wagner relaxation behaviors in the nanocomposite [Sharma *et al.* (2014)].The plots of tangent loss versus frequency at a few selected temperatures are shown in Figure 6.12(c) explained an increase in tan δ with decreasing frequency. This increment in the tangent loss with frequency due to space charge polarization occurs at an interface between

grains with insulating grain boundaries. The value of dielectric loss (tan δ) for BHF–BCT nanocomposite is found to be 1.45 at 100 Hz and 428 K.

6.7. Electrical and Impedance studies

Information about transport phenomenon as well as identification of the nature of the conduction mechanism of the samples was evaluated through electrical conductivity reliably data. Figure 6.13 demonstrates the variation of conductivity with frequency at a few selected temperatures of the BHF–BCT nanocomposite sintered at 1173 K for 8 h.

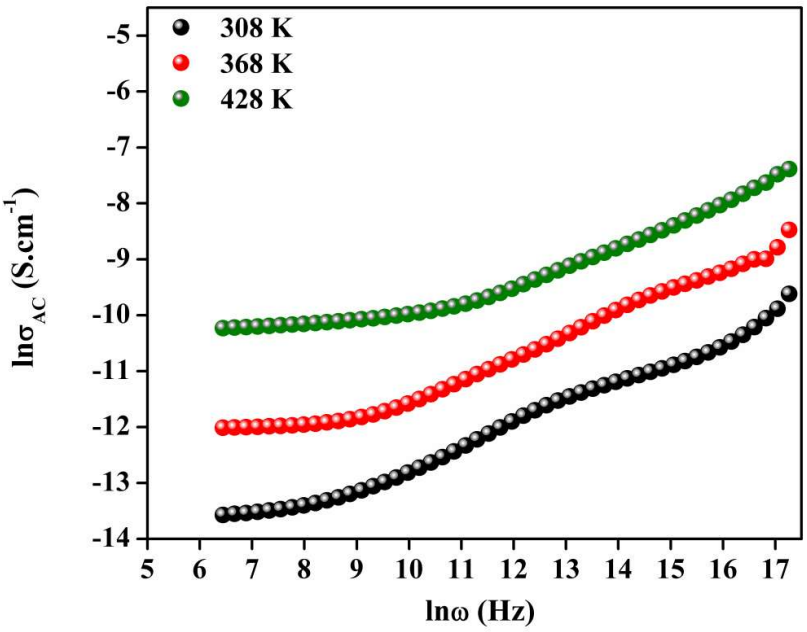

Figure 6.13 Frequency dependence of AC conductivity at few selected temperatures for BHF–BCT nanocomposite.

The total conductivity observed due to AC and DC contribution expressed by equation 6.4. The AC conductivity of the composite is analyzed by the Jonscher's power law as shown in equation 6.5.

$$\sigma = \sigma_{dc} + \sigma_{ac} = \sigma_{dc} + A\omega^s \quad (6.4)$$

$$\sigma_{ac} = A\omega^S \quad (6.5)$$

where, σ_{ac} and σ_{dc} are the ac conductivity and dc conductivity, respectively. A is the pre-exponential factor, ω is angular frequency, and s is the frequency exponent parameters [Singh *et al.* (2014)].The values of the exponent parameter (s) calculated from the plots of linear fitting and are found to be 0.81, 0.52 and 0.50 at 308, 368 and 428 K respectively. The value of s is less than one at different temperatures. The decrease in the value of s with an increase of temperature may be due to hopping charge mechanism which can be explained by Correlated Barrier Hopping (CBH) model, given by Elliot for crystalline oxide materials [Yadava *et al.* (2017)].

Figure 6.14 shows the variation of conductivity with the inverse of temperature at a few selected frequencies explain the increase in AC conductivity with increasing temperature. The temperature dependence of AC conductivity was strongly dominant at lower frequency region in comparison to higher frequency due to the existence of thermally activation process from the different localized state in the band gap [Slimani *et al.* (2019)]. Temperature dependence of AC conductivity obeys the Arrhenius law, given by the following equation 6.6.

$$\sigma = \sigma_0 \exp(\frac{-E_a}{kT}) \quad (6.6)$$

where, E_a is the activation energy for the thermally activated process, σ_0 is the pre-exponential factor, k is the Boltzmann constant and *T* is the absolute temperature. The activation energy calculated by the linear fitting was found to be 0.062, 0.061 and 0.046 eV at 1 kHz, 10 kHz, and 100 kHz, respectively. It is observed that the value of Ea slightly decreases with increasing frequency which corresponds to thermally activated process. The lower value of activation

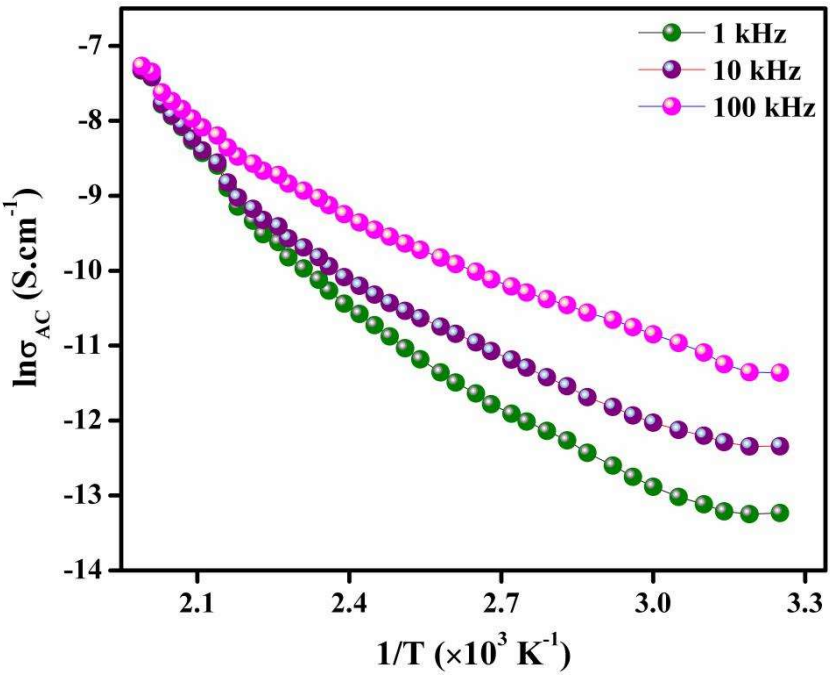

Figure 6.14 Variation of conductivity with inverse of temperature at few selected frequencies of BHF–BCT nanocomposite.

energy at higher frequency region may due to hopping charge mechanism which enhanced the conductivity of nanocomposite [Singh *et al.* (2015)].

The impedance of grains, grain boundaries, and electrodes of the composite was investigated by the complex impedance spectroscopy (CIS) technique (Cole-Cole plot). CIS is used for the estimation of resistance and capacitance corresponding to the grains and grain boundaries. A Cole-Cole plot is composed of two semicircles, in which one of the semicircles at lower frequency region is due to grain boundary contribution, and the other one at higher frequency region is due to grain contribution. The Cole-Cole plot of BHF–BCT nanocomposite ceramic at a few selected temperatures (308 – 428 K) is shown in Figure 6.15 reveals the

presence of one semicircular arcs. The expanded view of impedance plots at higher frequency region as

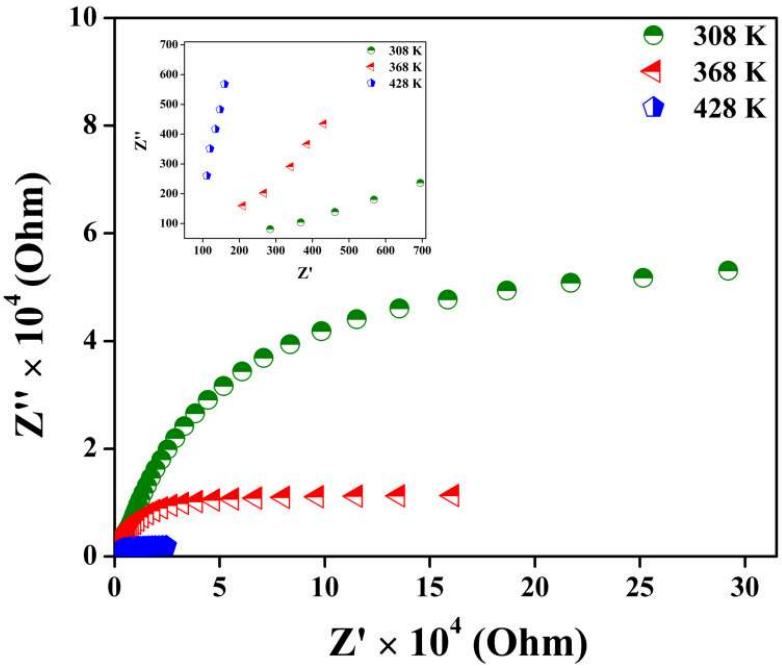

Figure 6.15 Impedance plots (z′ vs z″) of BHF–BCT nanocomposite at few selected temperature sintered at 1173 K for 8 h.

shown in inset indicates the intercept on the Z′ axis is not zero which explains the possibility of another semicircle at higher frequency is due to grain contribution. The non-zero intercepts on the Z′ axis are the grain resistance (R_g) and the semicircle observed at lower frequency represents the resistance of grain boundary (R_{gb}). No relaxation mechanism due to electrode effect could be identified by Cole-Cole plot in terms of frequency and temperature for BHF–BCT nanocomposite. The complex impedance (Z*) related with the real (z′) and imaginary (z″) impedance is given by the equation 6.7.

$$Z^{*}=\frac{1}{R_g^{-1}+i\omega C_g}+\frac{1}{R_{gb}^{-1}+i\omega C_{gb}}=Z'-iZ'' \quad (6.7)$$

Where

$$Z'=\frac{R_g}{1+(\omega R_g C_g)^2}+\frac{R_{gb}}{1+(\omega R_{gb}C_{gb})^2}$$

And

$$Z''=R_g\left[\frac{\omega R_g C_g}{1+(\omega R_g C_g)^2}\right]+R_{gb}\left[\frac{\omega R_{gb}C_{gb}}{1+(\omega R_{gb}C_{gb})^2}\right]$$

The grain resistance (R_g) of BHF–BCT nanocomposite is found to be 244,140,and 85 Ω at 308, 368 and 428 K, respectively and grain boundary resistance (R_{gb}) is found to be 2.9 × 10^5, 1.6 × 10^5 and 0.2 × 10^5 Ω, respectively at the same temperature. It is seen that the value of grains and grain boundaries resistance decreases with increasing temperature. The rapid decrease of grain boundaries resistance as compared to grain resistance with temperature shows semiconducting nature of grain boundaries [Yadava *et al.* (2016), Chen *et al.* (2006), Yadava *et al.* (2018)].

6.8. Conclusions

0.5BaFe$_{12}$O$_{19}$–0.5Bi$_{2/3}$Cu$_3$Ti$_4$O$_{12}$ (BHF–BCT) nanocomposite was synthesized by the chemical route at the sintering temperature 1173 K, which is much lower temperature compared to typical ceramic process for this class of materials and in a shortertime period of 8 hours. XRD patterns confirmed the existence of BHF and BCT phases in nanocomposite. The surface morphology, elemental compositions, and surface roughness were investigated by using SEM, EDX and AFM analysis, respectively. The highest value of dielectric constant BHF–BCT nanocomposite was found to be ε′ ~ 10.7 × 10^4 at 100 Hz and 428 K. The step like transition is observed in ZFC and FC curves displays maximum below T_M=170 K temperature and M–H hysteresis loop shows

ferromagnetic in nature of the BHF-BCT nanocomposite. The AC conductivity obeyed Jonscher's power law and decreasing of frequency exponent parameters (s) with increasing temperature can be explained by Correlated Barrier Hopping (CBH) mechanism. The impedance studies suggested that the nanocomposite has semiconducting grains and insulating grain boundaries.